# Electronic phase transitions and superconductivity in ferroelectric $Sn_2P_2Se_6$ under pressure

He Zhang,[1,2,*] Wei Zhong,[3,*] Xiaohui Yu,[1,2,4,†] Binbin Yue,[3,‡] and Fang Hong[1,2,4,§]
[1] *Beijing National Laboratory for Condensed Matter Physics, Institute of Physics, Chinese Academy of Sciences, Beijing 100190, China*
[2] *School of Physical Sciences, University of Chinese Academy of Sciences, Beijing 100190, China*
[3] *Center for High Pressure Science & Technology Advanced Research, 10 East Xibeiwang Road, Haidian, Beijing 100094, China*
[4] *Songshan Lake Materials Laboratory, Dongguan, Guangdong 523808, China*

(Received 27 February 2024; revised 24 April 2024; accepted 17 June 2024; published 26 June 2024)

Given the strong electron-phonon coupling observed during both ferroelectric (FE) and superconducting (SC) transitions, there is significant interest in investigating SC arising from FE instability. $Sn_2P_2Se_6$ has garnered considerable attention due to its unique FE properties. Here, we report on the electronic phase transitions and SC in this compound based on high-pressure electrical transport measurement, optical absorption spectroscopy, and Raman-based structural analysis. Upon compression, the conductivity of $Sn_2P_2Se_6$ increased monotonously, with an electronic phase transition occurring ~5.4 GPa, as evidenced by optical absorption spectroscopy. The insulating state was fully suppressed ~15 GPa, coinciding with the onset of SC ~15.3 GPa. A zero-resistance state was achieved from 19.4 GPa onwards, with SC exhibiting continuous enhancement under pressure. The SC behavior was further confirmed by the magnetic field effect, and it exhibited a critical temperature ($T_c$) of 5.4 K at 41.8 GPa and a zero-temperature upper critical field of 6.55 T. Raman spectra supported the structural origin of the electronic transition ~5.4 GPa, indicative of a transition from the paraelectric (PE) phase to the incommensurate phase—a distorted PE phase without symmetry change. Furthermore, a possible first-order phase transition was suggested during the semiconductor-metal transition ~15 GPa. Comparison with the high-pressure behavior of sister compounds $Sn_2P_2S_6$ and $Pb_2P_2S_6$, along with the low-temperature behavior of $Sn_2P_2Se_6$ at ambient pressure, suggests that SC in $Sn_2P_2Se_6$ likely emerges in a FE or polar metal state. In this paper, we highlight the versatile physical properties of FEs and motivate further investigation into the correlation between FE instability and SC in the $M_2P_2X_6$ family.

DOI: 10.1103/PhysRevB.109.214517

## I. INTRODUCTION

Ferroelectric (FE) materials play a pivotal role in both fundamental research and practical applications, with studies dating back over a century [1]. Among the most prevalent ferroelectrics are oxides such as $BaTiO_3$, $PbTiO_3$, and lead-free niobates. Over time, advancements in characterization techniques and theoretical modeling have significantly broadened our understanding of FE. Today, FE behavior can be elucidated using the formalism of quantum mechanical Berry phases [1]. In certain magnetic compounds, FE can arise from distinctive magnetic orderings, such as spiral spin ordering, and it can even coexist with ferromagnetic ordering [2]. Beyond oxide FEs, a plethora of FE materials have been discovered, ranging from metal chalcogenides [3,4] and polymers [5,6] to metal-organic frameworks [7] and two-dimensional bilayers with sliding behavior [8–10]. Benefiting from the switchable polarization, FEs find applications in diverse fields including sensing, energy conversion, FE random access memories, magnetoelectrics, and more.

In most cases, FE states manifest in materials exhibiting a band gap, as the presence of free electrons tends to screen long-range Coulomb forces, thereby disinclining the formation of a polar state [11]. Through chemical composition tuning or application of pressure, the paraelectric (PE)-to-FE transition can be effectively controlled, with the possibility of FE suppression leading to the emergence of a quantum PE phase or FE quantum critical point [12–14]. Given the strong electron-phonon coupling observed during the PE-to-FE transition and in Bardeen-Cooper-Schrieffer (BCS) superconductors, superconductivity (SC) may arise because of FE instability. A notable example is the doped $SrTiO_3$, near its FE quantum critical point, the SC is found to be mediated by the longitudinal hybrid-polar modes based on recent high-pressure experiments [15], and it can be enhanced by pressure-driven plastic deformation [16], which enhances the soft polar fluctuations, albeit authors of previous studies have suggested an unconventional SC mechanism [17]. Similarly, electron doping can induce FE soft mode instability in $LaOBiS_2$, leading to the emergence of SC alongside a distorted charge density wave [18]. Consequently, investigating the underlying exotic physics of FEs under external stimuli such as doping and pressure presents a compelling avenue of research.

$Sn_2P_2X_6$ ($X$ = S, Se) compounds have been identified as FE materials [4,19,20]. For $Sn_2P_2S_6$, it is a room-temperature

---

[*] These authors contributed equally to this work.

[†] Contact author: yuxh@iphy.ac.cn

[‡] Contact author: yuebb@hpstar.ac.cn

[§] Contact author: hongfang@iphy.ac.cn

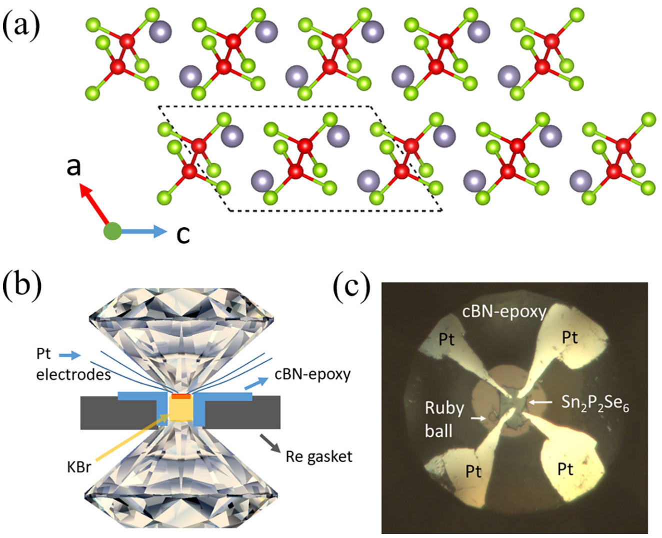

FIG. 1. The atomic structure of paraelectric phase ($P2_1/c$) of $Sn_2P_2Se_6$ and the sample loading in diamond anvil cell (DAC). (a) The atomic structure of $Sn_2P_2Se_6$ under ambient conditions. (b) Schematic representation of sample loading. (c) Photograph of the sample inside the DAC.

FE material with $T_c^{FE}$ at ∼337 K, while $T_c^{FE}$ reduces to ∼193 K in $Sn_2P_2Se_6$. Recent high-pressure investigations have revealed that $Sn_2P_2S_6$ transforms from the PE phase to a chiral $P2_1$ phase, exhibiting SC, likely associated with the presence of a flat band in the chiral phase [21]. Though $Sn_2P_2Se_6$ looks like its sister compound $Sn_2P_2S_6$, as $Sn_2P_2S_6$ and $Sn_2P_2Se_6$ share the same PE ($P2_1/c$) [as seen in Fig. 1(a)] and FE ($Pc$) structures, their PE-FE phase transition processes differ. Specifically, $Sn_2P_2Se_6$ undergoes an intermediate incommensurate (IC) phase transition, situated between the high-temperature PE phase and the low-temperature FE phase [20]. This IC phase exhibits an isosymmetric structure of the PE phase with a modulation wave vector $\mathbf{q} \approx 0.075$–$0.085\mathbf{c}^*$ (where $\mathbf{c}^*$ represents the reciprocal vector and is temperature dependent) [22]. While the PE-FE transition in $Sn_2P_2S_6$ is second order, it is first order in $Sn_2P_2Se_6$ during the IC-FE transition [22]. Given these distinctions, we investigated the electronic behavior of $Sn_2P_2Se_6$ by means of high-pressure transport, optical absorption, and Raman spectroscopies. $Sn_2P_2Se_6$ underwent an electronic phase transition ∼5.4 GPa, marked by a significant decrease in the optical band gap, likely attributable to the PE-IC phase transition, as indicated by the appearance of two new Raman modes in the low wave number region. The optical band gap was estimated to close ∼15 GPa, and then SC emerged ∼15.3 GPa, which was enhanced with pressure monotonously, and the SC critical temperature $T_c$ increased from ∼2.2 K at 15.3 GPa to 5.4 K at 41.8 GPa. Meanwhile, Raman signal was still detectable between ∼15 and ∼30 GPa, suggesting a possible first-order phase transition when the SC was presented. This hypothesis finds support in the distinct pressure-dependent behavior of $T_c$ observed below and above 30 GPa. Considering the similar effects on lattice structure between cooling and pressure, the phase transition under pressure may follow the sequence observed during the cooling process at ambient pressure. Consequently, the high-pressure phase may adopt a FE or polar metal state, with a similar behavior potentially existing in compressed $Sn_2P_2S_6$ [21]. In this paper, we elucidate the rich phase transitions in FE $Sn_2P_2Se_6$ under pressure and provide insights for future investigations into the correlation between FE instability and SC in such FE materials.

## II. EXPERIMENT

### A. Single-crystal sample

The $Sn_2P_2Se_6$ single crystal was supplied by Sixcarbon Technology (Shenzhen, China) and synthesized through chemical vapor transport reactions following procedures outlined in a previous study [23].

### B. High-pressure electric transport measurements

The four-probe electrical resistance measurement was carried out in a van der Pauw geometry under high pressure up to ∼43.5 GPa, and the experiment was conducted in a commercial cryostat (Janis Research) from 1.7 to 300 K by a Keithley 6221 current source and a 2182A nanovoltmeter (the testing dc current ranged from $10^{-7}$ to $10^{-4}$ A, dependent on the resistance of sample, the up limit of voltage is 1 eV, and the resistance was obtained in a Delta mode). To generate high pressure, two opposing anvils with 300 μm culets were placed in a BeCu alloy diamond anvil cell (DAC). A rhenium gasket with a thickness of 250 μm was compressed to ∼40 μm by the DAC, and a hole of ∼240 μm diameter was drilled using a laser. Subsequently, the entire indentation region was filled with a cBN-epoxy (15:1) mixture to efficiently avoid short circuits. The cBN-epoxy mixture was then compressed by the DAC to achieve a densified insulating layer. The remaining gasket region, which was not compressed by the DAC, was insulated using common AB glue. A sample hole of ∼100 μm was drilled by laser, and then a thin flake sample was loaded into the sample chamber, and a ruby ball was loaded to serve as an internal pressure standard. KBr was used as the pressure medium. Four Pt electrodes (4 μm thick) were manually placed and connected to the sample, welded directly with Cu testing wires. To minimize pressure gradients of the sample environment, a tiny sample with size of ∼30 μm ($W$) × ∼40 μm ($L$) × ∼5 μm ($H$) was cut from original bulk crystal (previously verified by Raman spectroscopy to ensure it is $Sn_2P_2Se_6$) and positioned in the center of the sample chamber. For illustration, a schematic of the DAC is provided in Fig. 1(b), while a photograph of the sample within the DAC is shown in Fig. 1(c). The raw resistance-temperature ($R$-$T$) data obtained from these measurements were utilized in this paper without any modifications.

### C. High-pressure spectroscopy measurements

High-pressure Raman spectra were acquired utilizing a Renishaw Micro-Raman spectroscopy system, which was outfitted with a second-harmonic Nd : YAG laser operating at 532 nm. To prevent sample overheating during measurement, the laser power was maintained at a relatively low level (1% of the laser power, ∼3 mW), with the laser power remaining constant throughout the experiment. For *in situ* high-pressure UV-VIS-NIR absorption spectroscopy, a

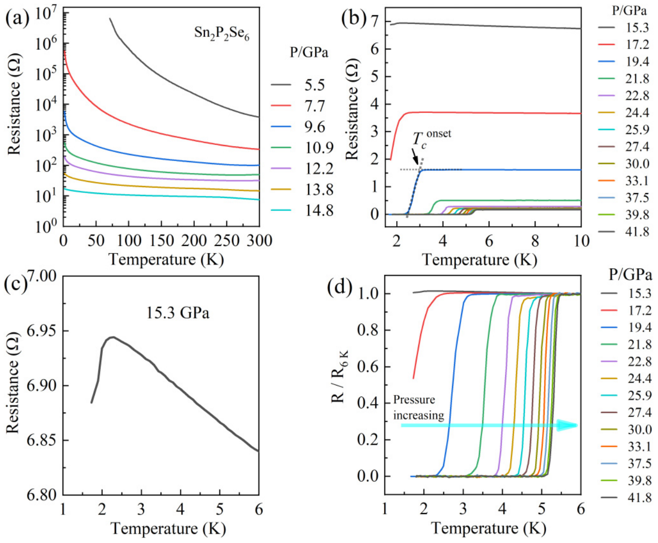

FIG. 2. Electrical transport properties of $Sn_2P_2Se_6$ under pressure. (a) Resistance-temperature (*R-T*) curves from 1.8 to 300 K under low pressure ranging from 5.5 to 14.8 GPa, indicating semiconducting behavior. (b) *R-T* curves from 15.3 to 41.8 GPa, highlighting superconducting (SC) transitions and the method used to determine the critical temperature $T_c$ ($T_c^{\text{onset}}$). (c) Zoom-in on the low-temperature region of the *R-T* curve at 15.3 GPa. (d) Normalized *R-T* curves at 6 K near the SC transition.

custom-designed spectroscopy system (Ideaoptics, Shanghai, China) was employed. A bromine-tungsten lamp served as the light source, spanning from 380 to 1700 nm. Our spectroscopy setup included a NOVA2S highly sensitive spectrometer operating in the 360–930 nm range and a NIR-1700 spectrometer operating in the 890–1700 nm range. In all spectroscopy measurements, type IIa diamond anvils with low fluorescent signals were utilized, with KBr serving as the pressure medium. Pressure was determined by observing the shift of R1-R2 ruby fluorescence lines [24].

## III. RESULTS AND DISCUSSION

The starting material, $Sn_2P_2Se_6$ is a semiconductor, and the initial resistance exceeds the detection limit of the experimental setup. By applying pressure, we were able to commence data collection for the *R-T* curve starting from ∼5.5 GPa. As illustrated in Fig. 2(a), at room temperature and 5.5 GPa, the resistance of the sample measures in the range of several thousand ohms, increasing by approximately three orders of magnitude at ∼75 K, indicative of an insulating ground state. However, further compression results in an increase in conductivity. The semiconductor behavior persists until 14.8 GPa, beyond which a slight decrease in resistance occurs below 2.2 K at 15.3 GPa, as depicted in Figs. 2(b) and 2(c). This characteristic drop in resistance signifies the onset of SC transition, with this behavior becoming more pronounced at higher pressures, culminating in a zero-resistance state observed at 19.4 GPa. The SC transition temperatures ($T_c$) shift to higher values as pressure increases, reaching 5.4 K at 41.8 GPa, the highest pressure investigated in this paper. To illustrate the trend of SC transitions clearly, the *R-T* curves are normalized and presented in Fig. 2(d). It is noteworthy that $T_c$ exhibits rapid increases at low-pressure ranges and appears to approach saturation ∼40 GPa. Previous room-temperature resistance measurements on $Sn_2P_2Se_6$ single crystal have also indicated significant changes under high pressure. The initial resistance of their sample was on a scale of $\sim 10^{10}\Omega$, decreasing to only several ohms above 15 GPa [25]. This observed change is largely consistent with our findings.

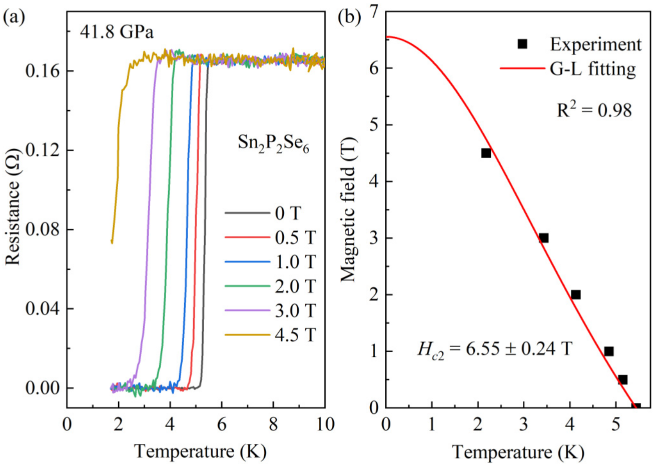

FIG. 3. Magnetic field effect on the superconducting transition in $Sn_2P_2Se_6$ at 41.8 GPa. (a) Resistance-temperature (*R-T*) curves at various magnetic fields from 0 to 4.5 T. (b) Relationship between upper critical field and temperature, along with the Ginzburg-Landau (G-L) fitting, yielding a fitting goodness of $R^2 = 0.98$.

To further corroborate the SC behavior, the magnetic field effect was investigated. The magnetic field was applied perpendicular to the layered structure of the original phase ($H \perp bc$ plane), as seen in Fig. 1(a). The SC transition regions under various fields are illustrated in Fig. 3(a). With increasing magnetic field strength, SC gradually diminishes, indicated by the shift of $T_c$ toward lower temperatures. Notably, the zero-resistance state is not observed at 4.5 T above 1.8 K. Following the extraction of $T_c$ from the *R-T* curves, a relationship between $T_c$ and the upper critical magnetic field $\mu_0 H_{c2}(T)$ was plotted, as seen in Fig. 3(b). To determine the upper critical magnetic field at zero temperature $\mu_0 H_{c2}(0)$, the relationship was fitted using the Ginzburg-Landau (G-L) equation $H_{c2}(T) = H_{c2}(0)[(1 - t^2)/(1 + t^2)]$ (where $t = T/T_c$, $T$ is the temperature, and $T_c$ is the SC critical temperature at zero field, fixed at 5.4 K) [26]. This fitting yielded a value of $\mu_0 H_{c2}(0) \approx 6.55$ T, which is lower than the BCS weak-coupling Pauli paramagnetic limit of $\mu_0 H_p = 1.84 T_c \approx 9.9$ T for $T_c = 5.4$ K, suggesting the absence of Pauli pair breaking [27].

To comprehend the electronic behavior prior to metallization, we utilized UV-VIS-NIR spectroscopy to ascertain the optical absorption edge and extract the optical band gap. Given the insulating behavior of the sample and poor conductivity under ambient conditions, electrical transport measurements yield limited information about its electronic structure. Figure 4(a) displays the optical absorption spectra of $Sn_2P_2Se_6$ single crystal under pressure. Near ambient condition, $Sn_2P_2Se_6$ single crystal exhibits a distinct absorption edge between 1.6 and 2.1 eV. By fitting the data with a Tauc relationship in the form of $(\alpha * h\nu)^{1/2} \propto (h\nu\text{-}E_g)$ [28,29], the optical band gap is determined to be ∼1.3 eV for the ambient

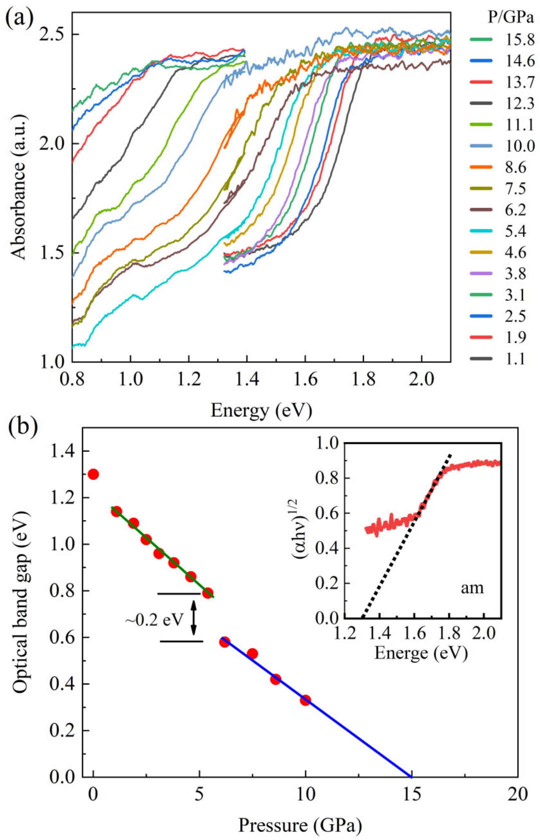

FIG. 4. The optical absorption spectra of $Sn_2P_2Se_6$ single crystal under pressure. (a) The UV-VIS-NIR absorption spectra of $Sn_2P_2Se_6$ single crystal from 1.1 to 15.8 GPa. (b) The relation between fitted optical band gap and pressure. Inset: The indirect band gap fitting under ambient conditions (am) by using a Tauc relationship in form of $(\alpha * h\nu)^{1/2} \propto (h\nu\text{-}E_g)$.

sample, as shown in the inset of Fig. 4(b). This initial indirect band gap is consistent with theoretical calculations [25]. Upon compression, the absorption edge shifts toward lower energy and broadens, making it difficult to discern the edge above 12.3 GPa. The band gaps at various pressures are depicted in Fig. 4(b). As pressure increases, the band gaps exhibit a monotonous decrease. At 1.1 GPa, the band gap reduces to 1.14 eV from the original 1.3 eV. Subsequently, the band gap vs pressure demonstrates a negative linear relationship until 5.4 GPa, beyond which a significant drop occurs, with the band gap decreasing to 0.33 eV at 10 GPa. Although determining the band gap becomes challenging from the broader absorption edge at higher pressure ranges, an estimation can still be made regarding when the sample may transition to a metallic state by extrapolating the band gap–pressure curve linearly. The critical pressure for band gap closure is ~15 GPa, a value that aligns well with the transport measurement. Notably, the abrupt drop in band gap ~5.4 GPa signifies an electronic phase transition and a potential structural phase transition, which will be explored further in subsequent discussions.

To investigate possible structural phase transitions, *in situ* high-pressure Raman spectroscopy was employed, and the results are presented in Fig. 5. Near ambient conditions (0.8 GPa), several relatively strong Raman vibration modes are observed, as depicted in Figs. 5(a) and 5(b), locating at ~150 $cm^{-1}$ (147 and 153 $cm^{-1}$, $A_g$), ~218 $cm^{-1}$ (the strongest mode, $A_g$), ~444 $cm^{-1}$ ($A_g/B_g$), ~456 $cm^{-1}$ ($A_g/B_g$), and ~483 $cm^{-1}$ ($A_g/B_g$), consistent with previous studies [25]. A diffusionlike background is observed close to the central peak (0 $cm^{-1}$) in the low-pressure range, and similar behavior was also reported in a previous Raman study [22]. The origin of this low-energy scattering background is currently unclear and may be attributed to possible short-range ordering (or fluctuations) in the PE phase. Upon compression, all these modes shift toward higher frequencies, albeit exhibiting different pressure dependencies to some extent, as shown in Fig. 5(a). At the first glance, there is no clear structural phase transitions up to ~30 GPa since all above main Raman modes persist until ~30 GPa. However, Raman peaks are suppressed above ~30 GPa, signaling a complete metallization. The critical pressure for the complete metallization aligns well with previous work [25], where the Raman peaks disappeared above ~29 GPa. Further insights can be gained by zooming into the low-wave-number region below 200 $cm^{-1}$. As seen in Figs. 5(b) and 5(c), there are some changes at low pressure which were not reported previously [25]. The noisy peaks are marked in Fig. 5(c), and these peaks come from the air and do not change with pressure [the background signal can also be well defined by the Raman spectrum (below ~150 $cm^{-1}$) at 33.5 GPa, as seen in Fig. 5(b)]. In Fig. 5(c), one clear feature is the intensity drop ~60 and ~150 $cm^{-1}$ at ~5 GPa. Another peak appears above ~5.6 GPa at ~128 $cm^{-1}$, as indicated by the green arrow in Fig. 5(c), and another mode ~112 $cm^{-1}$ is also presented above 6.5 GPa, as indicated by the gray arrow. The Raman change ~5.6 GPa is consistent with the optical absorption results, in which a drop of band gap is presented. Hence, there should be a local structural change which results in the electronic phase transition ~5.4 GPa. Furthermore, the pristine doublet peaks ~150 $cm^{-1}$ merge into one peak ~9.7 GPa (indicated by the pink arrow), and this mode shifts to ~175 $cm^{-1}$ at ~15 GPa. However, the intensity of this peak decreases quickly above ~15 GPa (indicated by the white arrow) and becomes broader and broader. The intensity drop and peak broadening are also consistent with previous findings [25]. The modes ~150 $cm^{-1}$ correspond to the internal Se-P-Se vibration modes in the $(PSe_3)^{2-}$ units [22,30,31]. Generally, $(PSe_3)^{2-}$ units are regarded as rigid bodies. However, under pressure, the intralayer and/or interlayer $(PSe_3)^{2-}$ units will connect with each other gradually, which causes the electron overlap (bonding) and metallization finally. Therefore, the broadening of this mode suggests the instability of $(PSe_3)^{2-}$ units due to the enhanced intermolecular interaction. It is worth noting that authors of previous work suggested a splitting ~150 $cm^{-1}$ above 11.6 GPa [25]. However, by comparing data quality, we believe their assertion may not be accurate, as their Raman signal was truncated ~150 $cm^{-1}$, making it difficult to distinguish the sample signal from the noisy background. The evolution of Raman modes under pressure is displayed in Fig. 5(d).

Considering the similar effects of temperature cooling and pressure (both shorten atomic-atomic distances and shrink

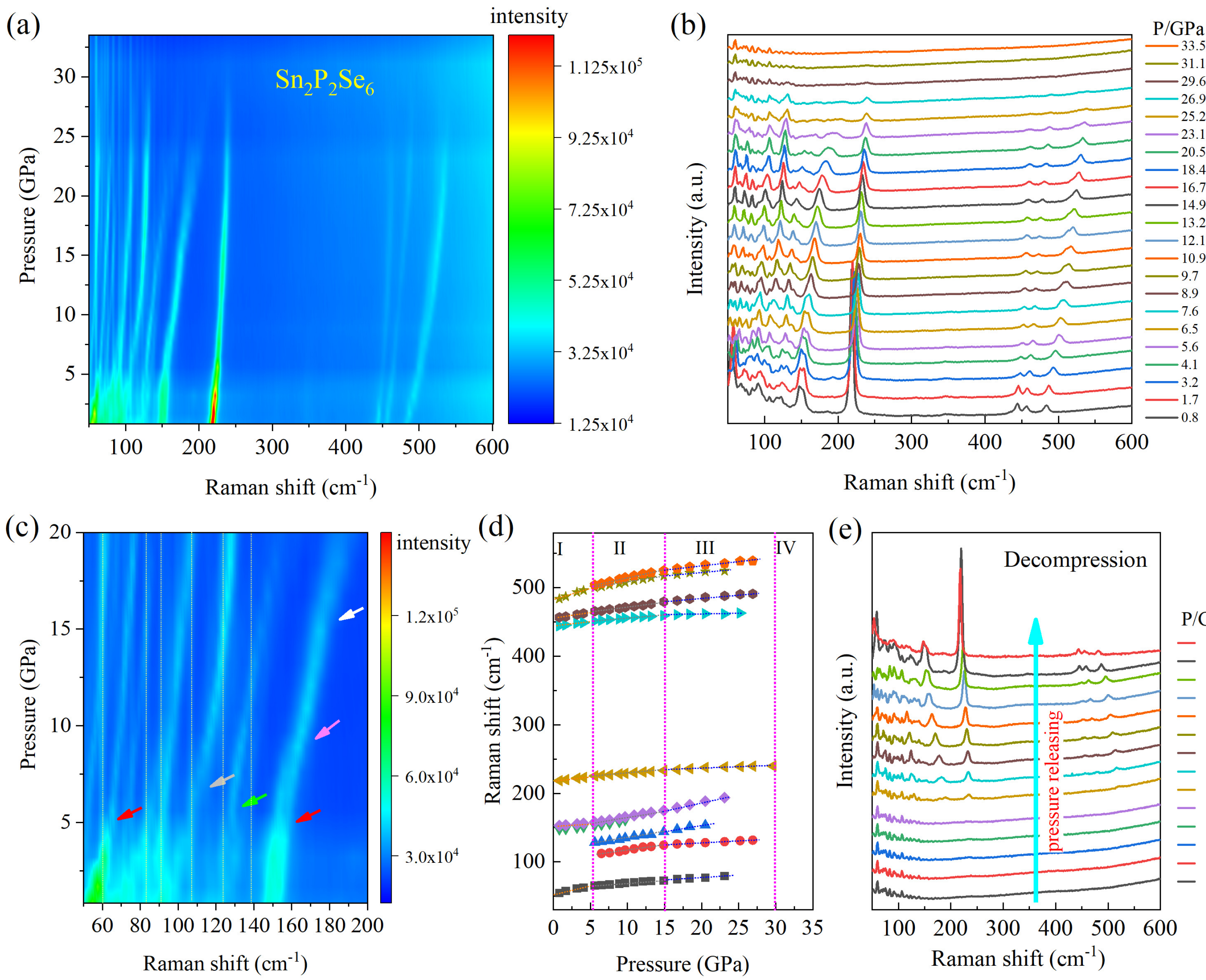

FIG. 5. The Raman spectra evolution with pressure in $Sn_2P_2Se_6$ single crystal. (a) Contour plot and (b) linear plot of the Raman spectra up to 33.5 GPa. (c) Zoomed-in region of Raman spectra at low wave numbers up to 20 GPa, with vertical dash lines indicating positions of background noisy peaks that remain constant with pressure. Arrows mark changes in Raman spectra. (d) Relationship between various Raman modes and pressure, proposing four regions for guidance. (e) Raman spectra collected during the decompression process, revealing a recoverable phase transition below ∼20.7 GPa.

the lattice), the phase transition ∼5.6 GPa could signify a transition to a low-temperature phase of $Sn_2P_2Se_6$. During this transition, in addition to the change in Raman intensity, the significant difference lies in the presence of two additional modes ∼128.8 and 112.2 cm$^{-1}$. Under ambient pressure, pristine $Sn_2P_2Se_6$ undergoes a phase transition from the PE to the IC phase before transforming to the FE phase *Pc*. This transition is an isosymmetric transition occurring at 221 K; both phases are in the form of a $P2_1/c$ structure, and it is a second-order phase transition, signaled by two additional modes located at 124 cm$^{-1}$ ($A_g$) and 107 cm$^{-1}$ ($A_g/B_g$) [22]. Accounting for the pressure-induced Raman shift, the two additional modes ∼128.8 and 112.2 cm$^{-1}$ at 5.6 and 6.5 GPa likely originate from the modes at 124 and 107 cm$^{-1}$ in the IC phase at 220 K. Hence, $Sn_2P_2Se_6$ could transform from the PE to the IC phase above ∼5.6 GPa at room temperature. Additionally, authors of an earlier study indicated a suppression of the IC and FE phases under external pressure [32], seemingly conflicting with our findings. However, this difference may stem from the instability of the PE phase itself under higher pressure. According to previous research [32], the phase transition temperature ($T_i$) of the PE-IC transition declines quickly with pressure; it probably reaches 0 K at only ∼1.5 GPa by extrapolating the $P$-$T_i$ relation linearly, and then the sample is in the PE phase from 0 to 300 K. Under higher pressure, the PE phase is no longer stable; on the contrary, the IC phase is perhaps favored by pressure. Given that SC is observed starting from 15.3 GPa while clear Raman signals are still collected, this behavior is typically associated with a mixture of phases during a first-order structural phase transition [33]. In other words, there could be a wide pressure window from ∼15 to ∼30 GPa during which the $Sn_2P_2Se_6$ sample undergoes a structural phase transition process: one phase remains the IC phase in an insulating/semiconducting state, while the other phase exhibits metallic and SC behavior. Such a first-order phase transition may align with the first-order IC-FE phase transition in the $Sn_2P_2Se_6$ sample at low temperature and ambient pressure. Therefore, it is plausible that $Sn_2P_2Se_6$ adopts a FE metal state at high pressure when the SC occurs. The characteristic of the first-order transition is further confirmed by the Raman spectra collected during the decompression process. As shown in Fig. 5(e), the Raman signal recovers below ~20.7 GPa, significantly lower than the critical pressure of ~30 GPa observed during the compression process. This observation also rules out the possibility of pressure-induced disproportionation and Se element-contributed SC, considering that $Sn_2P_2Se_6$ exhibits a similar $T_c$ to the Se element [34].

Compared with the high-pressure behavior in its sister compound $Sn_2P_2S_6$, some similarities emerge as well. There is an electronic phase transition in the PE phase ($P2_1/c$) of $Sn_2P_2S_6$, and the critical pressure is ~15 GPa, as revealed by the optical absorption results [21]. Meanwhile, the lattice parameters of the $P2_1/c$ phase also show some changes with pressure: the $\beta$ angle of the monoclinic structure exhibits a dip ~15 GPa, while the lattice parameter $a/b$ ratio shows a peak ~15 GPa [21]. These changes can be regarded as the features of an isostructure phase transition. Further compression leads $Sn_2P_2S_6$ to transform into a chiral $P2_1$ phase, which hosts a polar structure, potentially resulting in a FE state [35]. Hence, it is possible that $Sn_2P_2Se_6$ has a similar phase transition sequence to $Sn_2P_2S_6$, and $Sn_2P_2Se_6$ could show SC in a polar metal state (or even in a FE metal state). Another sister compound $Pb_2P_2S_6$ also has the same PE phase as $Sn_2P_2Se_6$ at room temperature. Authors of a recent high-pressure study have demonstrated that $Pb_2P_2S_6$ undergoes the insulator-metal and SC transitions above ~39 GPa, while remaining in its original phase without any phase transition [36]. This distinct behavior likely stems from the stable quantum PE behavior in $Pb_2P_2S_6$ [37,38]. The SC in $Pb_2P_2S_6$ could have a similar mechanism to that in quantum PE $SrTiO_3$ [17]. Further synchrotron x-ray diffraction experiments under high pressure are required to elucidate the detailed lattice structures and underlying mechanisms of SC in $Sn_2P_2Se_6$.

Based on the electrical transport measurement, optical absorption, and Raman spectra, we propose a concise electronic phase diagram for $Sn_2P_2Se_6$, as displayed in Fig. 6. At pressure lower than ~5.4 GPa, the sample is in a Semi-I state, maintaining the original monoclinic $P2_1/c$ structure. Between ~5.4 and ~15 GPa, the sample likely transitions to the IC phase due to changes in the local atomic environment, accompanied by an electronic phase transition. Near 15 GPa, the phonon mode ~175 $cm^{-1}$ of the sample begins to exhibit features of instability, the sample undergoes an insulator-metal transition, and shows SC transition below 2.2 K. Subsequently, the conductivity of the sample further improves, and SC is enhanced, as evidenced by the rapid increase in $T_c$ values. Between ~15 and ~30 GPa, Raman signals are still detectable despite the sample already becoming SC at low temperatures. The sample may undergo a first-order structural phase transition in this pressure range. Above 30 GPa, $T_c$ continues to increase with pressure, albeit at a slower rate. This behavior is also consistent with the Raman results, which shows that the sample experienced a complete metallization ~30 GPa, indicated by the disappearance of Raman signal. A detailed structural study is still necessary to elucidate the accurate lattice structures and their evolution under high pressure by using the synchrotron x-ray diffraction.

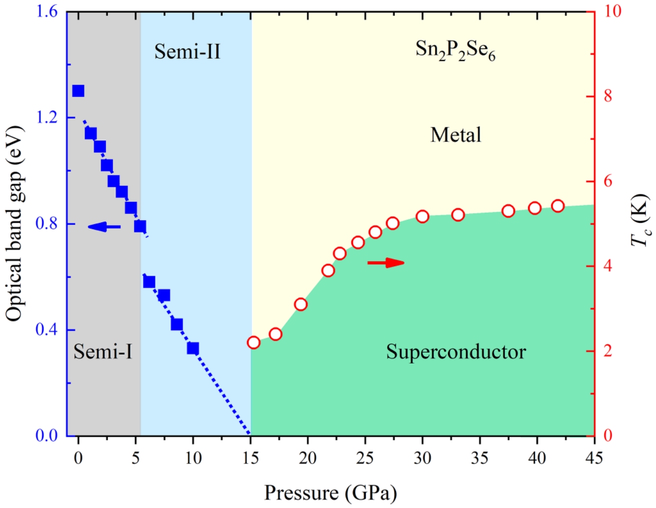

FIG. 6. Proposed electronic phase diagram for $Sn_2P_2Se_6$ under high pressure. Semi: semiconductor.

## IV. CONCLUSIONS

In summary, we report the SC and electronic behavior of the classic FE material $Sn_2P_2Se_6$ under pressure, utilizing a combination of electrical transport measurement, optical absorption, and Raman spectroscopy. At low pressure (<15.3 GPa), $Sn_2P_2Se_6$ exhibits insulating/semiconducting behavior. Subsequently, SC transition emerges at 15.3 GPa and is enhanced with further compression. The critical temperature ($T_c$) reaches 5.4 K at 41.8 GPa, and although the pressure-dependent increasing rate slows beyond 30 GPa, $T_c$ remains unsaturated. Optical absorption reveals an electronic phase transition ~5.4 GPa, confirmed by Raman results indicating its structural origin, likely due to the PE-IC phase transition. It is noteworthy that Raman signals persist up to 30 GPa despite the sample transitioning to a SC state above 15.3 GPa, suggesting a potential first-order structural phase transition between 15.3 and 30 GPa. The emergence of SC in $Sn_2P_2Se_6$ likely occurs in a FE/polar metal state, indicating its potential as a FE SC. In this paper, we show that $Sn_2P_2Se_6$ is sensitive to external pressure, and there are multiple phase transitions which determine the FE insulating state, metallic state (possible polar metal state), and even SC state. It inspires future comprehensive investigations into the correlation among FE/polar states, local structure, and SC.

## ACKNOWLEDGMENTS

This paper was supported by the National Key R&D Program of China (Grant No. 2021YFA1400300), the Major Program of National Natural Science Foundation of China (Grant No. 22090041), and National Natural Science Foundation of China (Grants No. 12374050, No 12004014, and No U1930401). Part of the experimental work was carried out at the Synergic Extreme Condition User Facility.

[1] J. F. Scott, Applications of modern ferroelectrics, Science **315**, 954 (2007).

[2] M. Fiebig, Revival of the magnetoelectric effect, J. Phys. D: Appl. Phys. **38**, R123 (2005).

[3] Z. Fei, W. Zhao, T. A. Palomaki, B. Sun, M. K. Miller, Z. Zhao, J. Yan, X. Xu, and D. H. Cobden, Ferroelectric switching of a two-dimensional metal, Nature (London) **560**, 336 (2018).

[4] Y. Vysochanskii, Ferroelectricity in complex chalcogenides $M'M''P_2X_6$ ($M'$, $M''$ - Sn, Pb, Cu, In, Cr; $X$ - S, Se), Ferroelectrics **218**, 275 (1998).

[5] A. J. Lovinger, Ferroelectric polymers, Science **220**, 1115 (1983).

[6] R. G. Kepler and R. Anderson, Ferroelectric polymers, Adv. Phys. **41**, 1 (1992).

[7] W. Zhang and R.-G. Xiong, Ferroelectric metal-organic frameworks, Chem. Rev. **112**, 1163 (2012).

[8] P. Meng, Y. Wu, R. Bian, E. Pan, B. Dong, X. Zhao, J. Chen, L. Wu, Y. Sun, Q. Fu *et al.*, Sliding induced multiple polarization states in two-dimensional ferroelectrics, Nat. Comm. **13**, 7696 (2022).

[9] K. Yasuda, X. Wang, K. Watanabe, T. Taniguchi, and P. Jarillo-Herrero, Stacking-engineered ferroelectricity in bilayer boron nitride, Science **372**, 1458 (2021).

[10] M. Wu and J. Li, Sliding ferroelectricity in 2D van der Waals materials: Related physics and future opportunities, Proc. Natl. Acad. Sci. USA **118**, e2115703118 (2021).

[11] W. Zhou and A. Ariando, Review on ferroelectric/polar metals, Jpn. J. Appl. Phys **59**, SI0802 (2020).

[12] J. M. Edge, Y. Kedem, U. Aschauer, N. A. Spaldin, and A. V. Balatsky, Quantum critical origin of the superconducting dome in $SrTiO_3$, Phys. Rev. Lett. **115**, 247002 (2015).

[13] S. Endo, K. Deguchi, and M. Tokunaga, Quantum paraelectricity in $KD_2PO_4$ and $KH_2PO_4$ under high pressure, Phys. Rev. Lett. **88**, 035503 (2002).

[14] R. Wang, N. Sakamoto, and M. Itoh, Effects of pressure on the dielectric properties of $SrTi^{18}O_3$ and $SrTi^{16}O_3$ single crystals, Phys. Rev. B **62**, R3577(R) (2000).

[15] C. Enderlein, J. F. de Oliveira, D. Tompsett, E. B. Saitovitch, S. Saxena, G. Lonzarich, and S. Rowley, Superconductivity mediated by polar modes in ferroelectric metals, Nat. Comm. **11**, 4852 (2020).

[16] S. Hameed, D. Pelc, Z. W. Anderson, A. Klein, R. J. Spieker, L. Yue, B. Das, J. Ramberger, M. Lukas, Y. Liu *et al.*, Enhanced superconductivity and ferroelectric quantum criticality in plastically deformed strontium titanate, Nature Mater. **21**, 54 (2022).

[17] M. N. Gastiasoro, J. Ruhman, and R. M. Fernandes, Superconductivity in dilute $SrTiO_3$: A review, Ann. Phys. **417**, 168107 (2020).

[18] T. Yildirim, Ferroelectric soft phonons, charge density wave instability, and strong electron-phonon coupling in $BiS_2$ layered superconductors: A first-principles study, Phys. Rev. B **87**, 020506(R) (2013).

[19] K. Moriya, H. Kuniyoshi, K. Tashita, Y. Ozaki, S. Yano, and T. Matsuo, Ferroelectric phase transitions in $Sn_2P_2S_6$ and $Sn_2P_2Se_6$ crystals, J. Phys. Soc. Jpn. **67**, 3505 (1998).

[20] T. Barsamian, S. Khasanov, V. S. Shekhtman, Y. M. Vysochanskii, and V. Y. Slivka, Incommensurate phase in proper ferroelectric $Sn_2P_2Se_6$, Ferroelectrics **67**, 47 (1986).

[21] B. Yue, W. Zhong, T. Wen, Y. Wang, H. Yu, X. Yu, C. Chen, J.-T. Wang, and F. Hong, Pressure-induced ferroelectric-to-superconductor transition in $SnPS_3$, Phys. Rev. B **107**, L140501 (2023).

[22] P. Van Loosdrecht, M. Maior, S. B. Molnar, Y. M. Vysochanskii, P. Van Bentum, and H. Van Kempen, Raman study of the ferroelectric semiconductor $Sn_2P_2Se_6$, Phys. Rev. B **48**, 6014 (1993).

[23] C. D. Carpentier and R. Nitsche, Vapour growth and crystal data of the thio(seleno)-hypodiphosphates $Sn_2P_2S_6$, $Sn_2P_2Se_6$, $Pb_2P_2Se_6$ and their mixed crystals, Mater. Res. Bull. **9**, 401 (1974).

[24] H. K. Mao, J. Xu, and P. M. Bell, Calibration of the ruby pressure gauge to 800 kbar under quasi-hydrostatic conditions, J. Geophys. Res. Solid Earth **91**, 4673 (1986).

[25] S. V. Ovsyannikov, N. V. Morozova, I. V. Korobeinikov, V. Haborets, R. Yevych, Y. Vysochanskii, and V. V. Shchennikov, Tuning the electronic and vibrational properties of $Sn_2P_2Se_6$ and $Pb_2P_2S_6$ crystals and their metallization under high pressure, Dalton Trans. **46**, 4245 (2017).

[26] J. A. Woollam, R. B. Somoano, and P. O'Connor, Positive curvature of the $H_{c2}$-versus-$T_c$ boundaries in layered superconductors, Phys. Rev. Lett. **32**, 712 (1974).

[27] A. M. Clogston, Upper limit for the critical field in hard superconductors, Phys. Rev. Lett. **9**, 266 (1962).

[28] J. Tauc, Optical properties and electronic structure of amorphous Ge and Si, Mater. Res. Bull. **3**, 37 (1968).

[29] J. Klein, L. Kampermann, B. Mockenhaupt, M. Behrens, J. Strunk, and G. Bacher, Limitations of the Tauc plot method, Adv. Funct. Mater. **33**, 2304523 (2023).

[30] M. Smirnov, J. Hlinka, and A. Solov'ev, Lattice dynamics and the ferroelectric phase transition in $Sn_2P_2S_6$, Phys. Rev. B **61**, 15051 (2000).

[31] I. Gregora and J. Hlinka, Directional dispersion of polar optical phonon frequencies in low-symmetry crystals: Raman studies on $Sn_2P_2S_6$, Ferroelectrics **267**, 237 (2002).

[32] A. Slivka, V. Kedyulich, and E. Gerzanich, Pressure effect on $Sn_2P_2Se_6$ type incommensurate crystals, Ferroelectrics **317**, 89 (2005).

[33] H. Zhang, W. Zhong, Y. Meng, B. Yue, X. Yu, J.-T. Wang, and F. Hong, Superconductivity above 12 K with possible multiband features in CsCl-type PbS, Phys. Rev. B **107**, 174502 (2023).

[34] Y. Akahama, M. Kobayashi, and H. Kawamura, Pressure-induced superconductivity and phase transition in selenium and tellurium, Solid State Commun. **84**, 803 (1992).

[35] G. H. Fecher, J. Kübler, and C. Felser, Chirality in the solid state: Chiral crystal structures in chiral and achiral space groups, Materials **15**, 5812 (2022).

[36] X. He, Z. Zhang, Z. Ding, S. Wang, C. Chen, X. Chen, Y. Zhou, C. An, M. Zhang, Y. Zhou *et al.*, Pressure-induced superconductivity in the metal thiophosphate $Pb_2P_2S_6$, Phys. Rev. Mater. **7**, 054801 (2023).

[37] I. Zamaraite, V. Liubachko, R. Yevych, A. Oleaga, A. Salazar, A. Dziaugys, J. Banys, and Y. Vysochanskii, Quantum paraelectric state and critical behavior in $Sn(Pb)_2P_2S(Se)_6$ ferroelectrics, J. Appl. Phys. **128**, 234105 (2020).

[38] R. Yevych, V. Haborets, M. Medulych, A. Molnar, A. Kohutych, A. Dziaugys, J. Banys, and Y. Vysochanskii, Valence fluctuations in $Sn(Pb)_2P_2S_6$ ferroelectrics, Low Temp. Phys. **42**, 1155 (2016).